Synergetic Adsorption of Polymers on Montmorillonite: Insights from Molecular Dynamics Simulations

Wenyuan Sun[†], Hongbo Zeng[‡] and Tian Tang*[,†]

[†]Department of Mechanical Engineering and [‡]Department of Chemical and Materials Engineering, University of Alberta, Edmonton, Alberta T6G 1H9, Canada

* Corresponding author, email: tian.tang@ualberta.ca, phone: +1-780-492-5467.

Abstract

In the treatment of industrial tailings, fine clay minerals are generally flocculated using polymer flocculants. Interestingly, applications of multiple types of polymers together were reported to enhance the flocculation, although the underlying mechanism was still unclear. In this work, a series of molecular dynamics simulations were performed to investigate the synergetic adsorption of two types of polymers on the basal surface of montmorillonite (Mt) in aqueous environment. Cationic chitosan molecules were first introduced, followed by the addition of either neutral polyacrylamide (PAM) or anionic Magnafloc (MF). A monolayer coating of chitosan was observed to form quickly on the Mt surface. The coating was stable and facilitated the subsequent adsorption of PAM or MF which by themselves did not show effective adsorption. Adsorption of PAM and MF showed different configurations. PAM could adsorb either directly on Mt or on chitosan, in the form of clusters or individual molecules. On the other hand, MF only adsorbed on chitosan, forming a two-layer structure above the Mt surface. Adding chitosan simultaneously with PAM or MF, instead of sequentially, did not change the characteristics of the adsorption. The synergetic adsorption of polymers was attributed to the interplay of electrostatic attraction between Mt and chitosan, hydrogen bonding between chitosan

1

23　and PAM, as well as electrostatic attraction between chitosan and MF. Together, the simulation

24　results allowed us to provide a mechanistic explanation for the experimentally observed

25　synergetic flocculation enabled by adding multiple polymers.

26

27　**Keywords: montmorillonite; chitosan; polyacrylamide; magnafloc; synergy; adsorption**

28

29　## 1. Introduction

30　　　Removing fine particles and recycling water from industrial wastewater especially tailings

31　have become an urgent need in the past decades (Wang et al., 2014). After the coarse fraction of

32　tailings segregated, a gel-like dispersion could form with very slow rate of consolidation

33　(Bakhshi et al., 1975), which made the removal of fine particles very difficult. As a result, the

34　tailings required long-term storage structures causing huge wasteland (Watson et al., 2010). The

35　slow dewatering of industrial tailings, continuous exploitation of natural resources, and growing

36　industrial manufacturing led to global shortage of clean water and lands (Moreno and Neretnieks,

37　2006; Watson et al., 2010). Consequently, environmental impacts brought by the fine particles

38　have been gaining more attention in recent years (Moreno and Neretnieks, 2006; Kaniki and

39　Tumba, 2019).

40　　　The fine particles in mineral tailings are mainly clay minerals such as kaolinite, illite, and

41　montmorillonite (Mt) (Omotoso and Mikula, 2004; Wang et al., 2014; Gorakhki and Bareither,

42　2015). It was found that basal surfaces of the clay minerals often carried permanent negative

43　charges, while the protonation of hydroxyl groups made the charge on the edge surfaces pH-

44　dependent (Bourg et al., 2007; Zeitler et al., 2017; Chen et al., 2020). The negative charges were

45　reported to be balanced by interlayer exchangeable cations, e.g., Na^+, K^+, Ca^{2+} (Theng, 2012).

2

46   Distributions of counter-ions and co-ions around the solid surface lead to the formation of the

47   diffuse electric double layer (EDL) (Israelachvili, 2011) which contributes to the stability of fine

48   clay minerals.

49   To reduce the stability of these mineral tailings, many chemical treatments were introduced

50   towards solid-liquid separation via flocculation (Long et al., 2006; Alamgir et al., 2012; Robert

51   et al., 2012; Nasim et al., 2018; Shaikh et al., 2018; Kang et al., 2019). Natural or synthetic

52   polymers and inorganic salts are considered as major types of flocculants. Many natural

53   polymers such as chitosan were shown to flocculate fine particles by adsorbing on the solid

54   surface through electrostatic attraction (Yang et al., 2011; Lu et al., 2016; Molatlhegi and Alagha,

55   2017). For example, Lu et al. (2016) reported that the zeta potential of particles in the

56   supernatants of mature fine tailings (MFT, concentrated dispersion of fine clay minerals

57   generated from water-based mining of oil sands) gradually increased from -38.6 mV to +30.2

58   mV when treated with increasing dosage of chitosan. Before reaching an optimum dosage (zeta

59   potential = 0 mV), as more chitosan was added, more particles were flocculated and settled

60   downwards, represented by the increasing initial settling rate (ISR) and decreasing turbidity of

61   the supernatant. On the other hand, hydrogen bonding (H-bonding) was also demonstrated to

62   facilitate the adsorption of polymers, such as neutral polyacrylamide (PAM) (Ji et al., 2013) as

63   well as its anionic derivatives Magnafloc (MF) (Ji et al., 2013), Zetag (Wang et al., 2016) and

64   poly (N-isopropyl acrylamide) (Zhang et al., 2017). These polymers have been extensively used

65   for solid-water separation since they are effective, inexpensive and have low toxicity. For

66   instance, Li et al. (2005) observed an increase in ISR when tailing samples were treated by

67   anionic HPAM (hydrolyzed PAM). It was proposed that H-bonding between the hydroxyl groups

3

68   of HPAM and clay mineral surfaces could induce bridging interactions between the clay mineral

69   particles, thus enhancing the phase separation.

70   Interestingly, instead of using a single type of polymers as flocculant, recent experimental

71   studies reported enhanced flocculation performance when two types of polymers were applied.

72   For example, in the work of Lu et al. (2016) the ISR reached as high as 10.26 m/h (meters per

73   hour) when the MFT were treated by MF at its optimum dosage, but the clarity of the supernatant

74   had no improvement compared with the untreated one. On the other hand, chitosan could render

75   a high clarity of the release supernatant, with turbidity of 15 NTU (nephelometric turbidity unit,

76   an indication of the relative clarity of water), but the highest ISR was only 1 m/h. Both high ISR

77   (7.7 m/h) and clear supernatant (turbidity of 71 NTU) were achieved by treating the MFT first by

78   MF and then by chitosan. Similar phenomena were also reported by other researchers (Zhang et

79   al., 2017).

80   Despite the observations from experiments, very limited theoretical work has been conducted

81   to investigate the mechanisms behind the solid-liquid separation, and as such there were

82   discrepancies between explanations proposed for the same observations (Theng, 2012). While

83   the adsorption of a single type of polymers onto clay mineral layers was examined by theoretical

84   simulations (Cygan et al., 2009; Cheng et al., 2015; Wei et al., 2017; Azevedo Rios Silva et al.,

85   2018; Ren et al., 2020), there has been no theoretical studies on the possible synergy between

86   multiple types of polymer flocculants in the vicinity of clay mineral surfaces. The effects of

87   polymer charges, adding sequence, and how the synergy is tied to the flocculation capability are

88   among the most interesting but unaddressed questions in the field.

89   To fill this gap, in the present work a series of molecular dynamics (MD) simulations were

90   performed to reveal the synergetic behaviors of two types of polymer flocculants when they were

4

91   added to the vicinity of a clay mineral surface. The clay mineral was represented by Mt with

92   negative charges. Three polymers were simulated: chitosan (cationic), PAM (neutral) and MF

93   1011 (anionic). Chitosan was added with either PAM or MF 1011 to study potential synergetic

94   effects. For comparison, simulations were also conducted on systems containing a single type of

95   polymers. As well, the effect of adding sequence was addressed by adding the two types of

96   polymers in different manners: simultaneously and sequentially.

2. Simulation methods

2.1 Molecular models

99   Mt belongs to the 2:1 mineral class, with a central sheet of octahedrally coordinated Al atoms,

100   sandwiched between two sheets consisting of SiO_4 tetrahedra (Viani et al., 2002). The unit cell of

101   Mt used in this work was based on the structure available in the American Mineralogist Crystal

102   Structure Database (Downs and Hall-Wallace, 2003), and their atomic coordinates were derived

103   by Viani et al. (2002). The unit cell parameters were $a = 5.18$ Å, $b = 8.95$ Å, $c = 15$ Å, and $\alpha = \beta$

104   $= \gamma = 90°$, where a, b and c were lattice constants in the three directions respectively, and α, β

105   and γ were the angles between the lattice sides. Hydrogen atoms were manually added to oxygen

106   atoms in the octahedral sheet. A neutral $2\times2\times1$ supercell was then built by closely stacking the

107   unit cells. Three Al atoms in octahedral sheet were isomorphically substituted by Mg, resulting

108   in a negative layer charge, as the tetrahedral sheets were less favorable to be substituted than the

109   octahedral sheet. The negative layer charge was neutralized by sodium ions in the system,

110   yielding a unit cell formula of $Na_{0.75}Si_8(Al_{3.25}Mg_{0.75})O_{20}(OH)_4$. The Na-Mt supercell was

111   subsequently expanded to a $16\times10\times1$ supercell (Figure 1a) to accommodate the polymers.

112   Chitosan, PAM, and MF 1011 were all modeled based on compounds in the PubChem

113   database (Kim et al., 2019). A 10-mer chitosan ($C_{60}H_{112}N_{10}O_{41}$, MW 1638 g/mol, Figure 1b) was

5

114 built and all amino groups were protonated. The protonation ratio represented the condition of

115 pH = 8; such a pH was typical in the treatment of process water as a result of adding alkaline

116 reagents such as sodium hydroxide (Allen, 2008). Previous experimental works (Wang et al.,

117 2006; Fernandes et al., 2012) also adopted the same pH value. MF 1011 was a sodium salt of

118 hydrolyzed PAM (Lu et al., 2016). MF ionomers with 9 units ($C_{27}H_{44}N_6O_{12}$, MW 641 g/mol,

119 Figure 1c) was simulated with a charge density of 33%. A neutral 10-mer PAM ($C_{30}H_{52}N_{10}O_{10}$,

120 MW 712 g/mol, Figure 1d) was used, corresponding to the same pH condition (Fraenkel and

121 Franconi, 1960; Grant et al., 2010).

122 **2.2 Systems simulated**

123 A total of nine systems (see Table 1) were simulated to study the adsorption of polymers on

124 the surface of Mt. System Mt-H$_2$O, with neutralizing sodium ions but without any polymers, was

125 first simulated to allow water and ions to equilibrate around the basal surface of Mt. Three

126 systems, namely Mt-CT, Mt-PAM, and Mt-MF, were simulated next to probe the adsorption of

127 single types of polymers on Mt. These simulations also allowed for comparison with systems

128 that involve two types of polymers. In each of these three systems, twelve molecules of chitosan,

129 PAM or MF were introduced into the equilibrated aqueous solution above the Mt, forming a

130 3×2×2 array as shown in Figure 1a. The number of sodium ions was adjusted accordingly in each

131 system to maintain charge neutrality.

132 The following two simulations, Mt-(CT-PAM) and Mt-(CT-MF), were performed where

133 chitosan and PAM (in system Mt-(CT-PAM)) or chitosan and MF (in system Mt-(CT-MF)) were

134 added simultaneously above the clay mineral surface. The polymers were also added in the form

135 of a 3×2×2 array as shown in Figure 1a, with one type of polymers forming the 3×1×2 array on

136 the left and the other on the right. Lastly, to study the effect of adding sequence, twelve MF

137   molecules were placed above the Mt previously coated by chitosan, which resulted from the Mt-

138   CT simulation. This formed the initial configuration for system (Mt-CT)-MF. System (Mt-CT)-

139   PAM was constructed in the same manner, with MF replaced by PAM. One additional system,

140   (Mt-PAM)-CT, was simulated by using the configuration of system Mt-PAM at 100 ns and

141   adding twelve chitosan molecules, in the form of a $3\times2\times2$ array, above the Mt surface pre-coated

142   by PAM.

143   **2.3 Simulation details**

144   The force field parameters for Mt were adopted from the CLAYFF force field (Cygan et al.,

145   2004; Pouvreau et al., 2017). CLAYFF was designed for clay mineral models and has a good

146   compatibility with organic force fields. The partial charges of all the atoms remained the same as

147   in CLAYFF, however the potentials for van der Waals were converted into forms compatible

148   with GROMOS96 53A6 (Oostenbrink et al., 2004). Validation of the force field parameters is

149   given in Supporting Information (SI, Section S1). Force field parameters for chitosan, PAM and

150   MF were first obtained from the GlycoBioChem PRODRG server (Schüttelkopf and Van Aalten,

151   2004) by submitting the initial atomic coordinates and invoking the GROMOS96 force field

152   parameter set 53A6. The partial atomic charges were then manually adjusted based on the

153   density functional theory (DFT) calculation from Gaussian 16 (Frisch et al., 2016). More details

154   about the calculation of partial atomic charges of the three types of polymers are given in the SI

155   (Section S2).

156   All MD simulations were carried out using GROMACS (Berendsen et al., 1995; Pronk et al.,

157   2013; Abraham et al., 2015) with periodic boundary conditions applied in all directions. As such,

158   the polymers were essentially located between two basal surfaces of Mt. Water and sodium ions

159   were first introduced and equilibrated for 2.5 ns in NPT ensemble. Then, polymers were solvated

160 into the equilibrated Mt-H_2O system with the number of sodium ions adjusted accordingly. Each

161 system was subjected to a geometrical optimization followed by NPT equilibration. Due to the

162 different nature and strength of interactions between the polymers and Mt, different systems

163 required different time to reach equilibrium (see Table 1, more details in SI Section S3).

164   The temperature was controlled at 300 K by Nose-Hoover thermostat (Nosé, 1984; Hoover,

165 1985), and pressure was controlled at 1 bar by Parrinello–Rahman barostat (Parrinello and

166 Rahman, 1981). Leap-frog algorithm (Hockney et al., 1974) was used for the integration of

167 equations of motion, with a time step of 1 fs. The bonds within all molecules were constrained

168 by LINC algorithm (Hess et al., 1997) except those in H_2O which were constrained by SETTLE

169 (Miyamoto and Kollman, 1992). Long-range electrostatic interactions were handled by particle

170 mesh Ewald (PME) method (Darden et al., 1993).

171 **3. Results and discussion**

172 **3.1 Adsorption of a single type of polymers**

173   The final configurations of systems Mt-CT, Mt-PAM, and Mt-MF are displayed in Figure 2.

174 In Figure 2a, the adsorbed chitosan molecules formed a stable monolayer coating on each Mt

175 surface. In Figure 2b, only the chitosan molecules adsorbed on the upper surface are shown,

176 which adhered to the surface in a dispersed manner. Detailed examination of the adsorption sites

177 revealed a close correlation with the locations of the isomorphic substitutions (see more details in

178 SI, section S3). Interestingly, Willemsen et al., 2019 reported the anticorrelation between the

179 adsorption sites of phthalate esters with locations of isomorphic substitutions, which was caused

180 by the hydrophobic nature of phthalate esters and the resulting preference of adhering to

181 uncharged patches. Different from chitosan, PAM molecules as shown in Figure 2c and Figure

8

182   2d tended to form clusters among themselves. All the MF molecules remained dispersed in bulk

183   water without adsorbing to the clay mineral surfaces, as shown in Figure 2e and Figure 2f.

184

185

186   The vertical distances (D), as a function of time, between the center of geometry (COG) of

187   Mt and the COG of one representative polymer molecules in each of the three systems are shown

188   in Figure 3. The results for the other polymer molecules in each system are shown in SI (Section

189   S3), which shared similar characteristics. All chitosan molecules moved towards Mt quickly,

190   with a fast decay in D in the first 2 ns, and then stayed on the surfaces without detaching again.

191   The adsorption of chitosan was driven by the strong electrostatic attraction between the

192   positively charged chitosan and the negatively charged Mt. Meanwhile, the electrostatic

193   repulsion among the chitosan molecules caused them to adsorb separately on the surface and

194   form a monolayer coating. Consistent with the snapshots shown in Figures 2e and 2f, MF

195   molecules were dispersed in the bulk without adsorption, and the value of D was above 2 nm for

196   most of the simulation time. The electrostatic repulsions between the negatively charged MF and

197   Mt as well as among MF molecules kept them apart from approaching each other. The

198   adsorption of PAM molecules was much slower and weaker, as D was below 1 nm at ~10 ns for

199   the first time and increased again. Throughout the simulation, D underwent large fluctuations,

200   corresponding to frequent exchange between adsorbed and desorbed states. Such unstable

201   adsorption was driven by the H-bonds between amides of PAM and bridging O in the basal

202   surfaces of Mt. In addition, PAM could adsorb on Mt in the form of either a single molecule or

203   an aggregate. More details on determining the aggregation state of PAM molecules are given in

204   SI (Section S3). For example, the representative PAM molecule shown in Figures 3 was

9

205 adsorbed as a single molecule (square symbols) at around 10 ns, 25 ns, and 60 ns, whereas

206 between 90 ns and 105 ns it was adsorbed as a molecule in an aggregate ("×" symbols).

207   Quantitative analysis on H-bonding provided further assessment on the characteristics of

208 PAM adsorption. The total numbers of H-bonds between PAM and Mt (n_H) was calculated and

209 then normalized with respect to the number of donor/acceptor pairs available (N_0, more details in

210 SI, section S4). This ratio, $p = n_H/N_0$, represented the percentage of available donor/acceptor

211 pairs that actually contributed to H-bonding. The same calculation was done for the H-bonding

212 between PAM molecules, and both results are shown in Figure 4. In the first 8 ns, p between

213 PAM and Mt remained zero while the number among PAM molecules quickly increased,

214 corresponding to the clustering of PAM molecules in the bulk solution. The value of p among

215 PAM molecules fluctuated steadily between 7% and 16% for the rest of the simulation time,

216 indicating the stability of the formed aggregates. Meanwhile, participating percentage of

217 donor/acceptor pairs between PAM and Mt remained less then 2%, and frequently reduced to

218 zero, suggesting reversible adsorption/desorption of the PAM molecules. The increases of p

219 between PAM and Mt from 50 to 80 ns, and from 90 to 110 ns, were caused by PAM adsorption

220 in either individual or aggregated forms, and examples are shown in the snapshots in Figure 4.

221 **3.2 Adsorption of simultaneously added polymers**

222   The configurations of systems Mt-(CT-PAM) and Mt-(CT-MF) at different time are shown in

223 Figure 5. Consider first system Mt-(CT-PAM) in Figure 5a-d. At $t = 3$ ns (Figure 5b), all the

224 chitosan molecules became adsorbed on Mt while the PAM molecules were still in the bulk.

225 Because chitosan molecules were initially placed on the right side of the simulation box, the

226 adsorption occurred on the right side as well. That is, the chitosan molecules found the shortest

227 path to form contact with Mt. As the simulation continued, the chitosan molecules started

10

228   spreading over the entire Mt surface, forming a thin monolayer similar to what was seen in

229   Figure 2a. Meanwhile, several PAM molecules started adhering to the adsorbed chitosan while

230   some of them also adsorbed directly on Mt surrounded by chitosan molecules, as illustrated in

231   Figure 5c. At the end of the simulation (Figure 5d), all the polymers were adsorbed, and the

232   PAM molecules conformed much better to the surface than in Figure 2b where a bulky PAM

233   cluster adhered to the surface with significant exposure to the solvent. Clearly, the presence of

234   chitosan greatly enhanced the adsorption of PAM.

235   The behaviors in system Mt-(CT-MF) as depicted in Figure 5e-h were similar to those in

236   system Mt-(CT-PAM): the process also began by attachment and subsequent spreading of

237   chitosan, followed by the adsorption of MF via chitosan, and all the polymer molecules were

238   adsorbed at the end. The enhancement of MF adsorption was significant, considering that in

239   Figure 2c all MF molecules were dispersed in the bulk with no adsorption at all. Compared with

240   system Mt-(CT-PAM), there were a few differences in system Mt-(CT-MF). First of all, in the

241   initial stage of the simulation some chitosan could be "captured" by the negatively charged MF

242   in the bulk (see Figure 5f at $t = 3$ ns) and their adsorption to Mt was delayed (not until $t = 30$ ns

243   in Figure 5g where the clustered chitosan and MF adsorbed together). On the contrary, for

244   system Mt-(CT-PAM), there was little interaction between the positively charged chitosan and

245   neutral PAM before surface adsorption of chitosan. Secondly, while PAM molecules could

246   adsorb on Mt via two modes (directly and indirectly through chitosan bridges), all MF adsorption

247   occurred via binding with chitosan.

248   The different modes of adsorption could be further confirmed by the vertical distances (D)

249   between the COG of polymer molecules and COG of Mt, as plotted in Figure 6, against

250   simulation time. Results are only shown for one chitosan (labeled as CT_1), two PAM molecules

11

251 (labeled as PAM_1, PAM_2) in Mt-(CT-PAM), and one MF molecule (labeled as MF_1) in Mt-

252 (CT-MF), while the rest are given in the SI (Section S3). Chitosan in both systems displayed the

253 same trend as CT_1: D reduced to about 0.5 nm after 2 ns and remained constant, corresponding

254 to fast, direct and stable adsorption. All MF in Mt-(CT-MF) also exhibited the same mode of

255 adsorption, as D reduced to 1.5 nm at ~25 ns in Figure 6 and was stable afterwards. This larger

256 steady-state value of D, compared to chitosan (0.5 nm), suggests that MF adsorbed on top of the

257 chitosan monolayer and could not move closer to Mt. The fast movement and stable coating of

258 chitosan on Mt were due to the strong electrostatic attraction between positively charged

259 chitosan and negatively charged Mt. Such attraction also existed between chitosan and negative

260 MF, while MF and Mt were mutually repulsive. These interactions determined the mode of

261 adsorption in Mt-(CT-MF), where chitosan molecules were sandwiched between Mt and MF

262 serving as bridges.

263   PAM in system Mt-(CT-PAM) displayed two modes of adsorption. The first was represented

264 by PAM_1, for which D maintained a value of ~0.5 nm after 25 ns, representing a stable

265 adsorption directly on the surface of Mt. Contrary to PAM_1, PAM_2 displayed a more dynamic

266 motion. At ~20 ns, it approached Mt with D staying at ~1.5 nm for about 10 ns. During this time,

267 PAM_2 adsorbed to Mt via a chitosan bridge, similar to MF molecules in Mt-(CT-MF).

268 Afterwards D increased rapidly corresponding to departure of PAM_2 from Mt. It adhered to Mt

269 again after 45 ns with D fluctuating between 0.5 nm and 1.5 nm. Such fluctuation represented the

270 switch between the two adsorption modes: directly on Mt and adsorption via chitosan.

271   Overall charge neutral PAM molecules interacted with chitosan via the formation of H-bonds

272 between the hydroxyl groups of chitosan and amides of PAM. The ability of PAM to form H-

273 bonds with chitosan as well as with Mt led to both direct adsorption and indirect adsorption via

12

274   chitosan bridges. Similar to Figure 4, the percentages of available donor/acceptor pairs that

275   contributed to H-bonding, p, were calculated for system Mt-(CT-PAM) and shown in Figure 7.

276   From 0 to 10 ns, p value was highest among PAM molecules, slightly above zero between

277   chitosan and PAM, and zero between PAM and Mt. Therefore, similar to system Mt-PAM,

278   during the initial stage clustering of PAM was favored and no immediate adsorption onto Mt was

279   observed. Meanwhile, PAM started interaction with the adsorbed chitosan layer. From 10 to 25

280   ns, p among PAM molecules reduced to one half of the original value while p between PAM and

281   chitosan increased. H-bonds between PAM and Mt also began to form. The results suggested

282   conversion of some PAM-PAM H-bonds to PAM-chitosan and PAM-Mt H-bonds. PAM

283   aggregates previously formed in the bulk broke into smaller ones to facilitate the adsorption.

284   From 25 to 80 ns, the value of p among PAM first increased and then decreased, indicating the

285   reversibility of PAM aggregation. The value of p between PAM and chitosan fluctuated at a

286   lower level than the curve between PAM and Mt which increased significantly, suggesting that

287   direct adsorption was more favorable compared to indirect adsorption via chitosan bridges.

288   Comparing the data in the last 20 ns of Figure 4 and Figure 7, there was a 50% reduction in

289   the p value among PAM molecules, from ~12% in Figure 4 to ~6% in Figure 7. Meanwhile,

290   there was a 20-fold increase in p between PAM and Mt, from ~0.2% in Figure 4 to ~4% in

291   Figure 7. Chitosan not only served as bridges for the indirect adsorption of PAM, but also

292   suppressed the aggregation of PAM molecules and greatly promoted the direct adsorption of

293   PAM on Mt. As PAM molecules were brought closer to Mt via the chitosan bridges, their short-

294   ranged attractions with Mt were enabled, which drove them to continue moving towards Mt until

295   direct H-bonding was established.

13

3.3 Adsorption of sequentially added polymers

The configurations of systems (Mt-CT)-PAM and (Mt-PAM)-CT at different time are shown in Figure 8. Consider system (Mt-CT)-PAM as shown in Figure 8a-d, the adsorption showed no difference compared with system Mt-(CT-PAM) shown in Figure 5a-d. Since chitosan moved much faster towards Mt than PAM, adding chitosan first or adding them simultaneously did not affect the adsorption. Similar observations were found for system (Mt-CT)-MF (more details in SI Section S3).

What is more interesting is system (Mt-PAM)-CT where chitosan molecules were added to Mt-PAM with an adsorbed PAM cluster on Mt. Even though in this case PAM adsorption had already occurred before the introduction of chitosan, the stronger long-range electrostatic attraction between chitosan and Mt still drove the formation of a chitosan monolayer on Mt at the end of the simulation (Figure 8h), which was similar to systems (Mt-CT)-PAM and Mt-(CT-PAM). During this process, however, the PAM aggregate was never "released" from the surface into the bulk. Instead, chitosan maintained their interactions with PAM while forming intimate contact with Mt (see Figure 8f and 8g). Consequently, the PAM aggregate was anchored to the vicinity of the Mt, gradually allowed chitosan to insert between PAM and Mt, and finally adsorbed on the formed chitosan monolayer. PAM initially adsorbed as individual molecules (Figure 8e) remained adsorbed directly, and were not disrupted by chitosan.

3.4 Implications

As discussed in Section 3.1, chitosan molecules adsorbed quickly and formed a monolayer coating on Mt. Though the two clay mineral surfaces could not be brought together by chitosan due to the application of periodic boundary conditions, the ability of chitosan to bridge two bare clay mineral surfaces were proved in other contexts such as fabrication of nanocomposites

14

319   (Razmimanesh et al., 2015; Wang et al., 2015). In industrial tailings, a clay mineral particle

320   coated by chitosan could have neutral or even reversed zeta potential (Lu et al., 2016; Zvulunov

321   et al., 2019). As such, it could attract another bare clay mineral surface, flocculating them

322   together. However, if both particles were coated by chitosan and possessed positive surface

323   charges, the electrostatic repulsion between them would hinder their aggregation and limit the

324   growth of flocs, as illustrated in Figure 9a. As a result, it can be hypothesized that the flocs will

325   settle slowly due to their small size. Since the adsorption of chitosan is highly stable, clay

326   mineral particles captured in the flocs are less likely to be released back to the supernatant,

327   resulting in high clarity. This result is consistent with the experimental observation that the ISR

328   of chitosan or other cationic polymers treated wastewater/tailings showed a low ISR but high

329   clarity of supernatant (Lu et al., 2016; Zhang et al., 2017).

330   PAM molecules by themselves could adsorb on Mt, but the adsorption tended to be in the

331   form of an aggregate and was not stable. It could then be inferred that in macroscopic systems,

332   PAM alone might induce multi-layer adsorption with reversible desorption. Two clay mineral

333   particles with adsorbed PAM can further aggregate since the neutral PAM does not introduce

334   repulsion between them while allowing for H-bonding among the adsorbed PAM molecules.

335   This interaction mechanism can lead to large flocs that settle quickly in clay mineral dispersion,

336   consistent with experimental observation (Wang et al., 2010; Zhang et al., 2017). On the other

337   hand, the unstable adsorption can allow a large amount of clay minerals to be released back to

338   the bulk solution, as illustrated in Figure 9b. Consequently, the clarity of clay mineral dispersion

339   is expected to be low, which was observed by various experiments (Liu et al., 2016; Lu et al.,

340   2016).

15

341   In experiments, when two types of flocculants were added simultaneously, the floc size

342   displayed a two-stage growth (Wang et al., 2016) which was consistent with the two-step

343   adsorption as shown in the system Mt-(CT-PAM). Regardless of the adding sequence, our

344   simulations showed that the cationic polymers formed the most intimate adsorption on the clay

345   mineral followed by the neutral polymers. The cationic coating stabilized the adsorption of

346   neutral flocculants, while the outer layer of neutral polymers promoted the local attractive forces

347   such as H-bonding, bridging them together to form larger aggregates, as illustrated in Figure 9c.

348   Compared with the application of a single type of flocculants, such synergetic effect is expected

349   to not only increase the ISR by forming larger clay mineral aggregates but also enhance the

350   clarity of the supernatant by reducing the number of bare clay mineral particles in it. The result is

351   consistent with previous reports where the addition of two types of polymers showed both high

352   ISR and clarity (Lu et al., 2016; Zhang et al., 2017). The synergetic effect was also present when

353   a cationic and an anionic flocculants were added, as our simulations showed a similar two-stage

354   adsorption process for chitosan and MF. The bonding strength between chitosan and MF was in

355   fact larger than that between chitosan and PAM. Although if two particles both possessed an

356   outer MF layer they would repel, in macroscopic systems it is possible to have multi-layer

357   adsorption in the form of CT-MF-CT, CT-MF-CT-MF, etc., which would allow particles with

358   opposite apparent surface charges to aggregate. To the best of our knowledge, this is the first

359   theoretical work that investigated the adsorption of polymer flocculants from molecular level and

360   accounted for the different flocculation behaviors. The results provided molecular evidence that

361   applying polymers with different charge properties would promote the flocculation and the

362   applying sequences had limited influence. Our findings may also be of value to other

16

363   applications, such as capture and storage of organic resources, as well as the design of clay

364   polymer nanocomposite.

365   **3.5 Limitations**

366   In the present work, the basal surface of Mt was chosen as a representative clay mineral

367   surface, while actual clay particles also contain edge surfaces and interlayers. When it comes to

368   polymer flocculation, the likelihood of adsorption of polymer flocculants in the interlayers is

369   expected to be low. This is because the interlayer spacing is on the order of nanometers (Suter et

370   al., 2011), which is difficult to accommodate polymer flocculants whose molecular mass is

371   usually in the range of 10^6-10^7 g/mol (Alamgir et al., 2012; Lu et al., 2015). The relative

372   importance of basal and edge surfaces is an interesting but complex problem. For example,

373   characterization results from XRD and SAXS showed preferential interactions of polymers with

374   basal surface (Li et al., 2019; Willemsen et al., 2019), with edge surface (Song and Sandí, 2001),

375   or comparable affinities to both surfaces (Ngnie et al., 2018). The distinct results were likely

376   caused by the different charges and terminating groups on the basal and edge surfaces, different

377   polymer properties, as well as different solution chemistries (e.g. pH, ions). Since the focus of

378   this study was to investigate the synergy of polymer adsorption arising from interactions such as

379   electrostatics and hydrogen bonding, the use of a single-layer basal surface served the purpose.

380   The mechanism discovered in this work should also be applicable to an edge surface if its

381   interactions with the polymer flocculants were governed by the same types of intermolecular

382   forces, although confirmation of this hypothesis would require addition investigations.

383   In addition to Mt, other types of clay minerals also exist in industrial tailings (Theng, 2012),

384   for example, kaolinite and illite. Kaolinite is a 1:1 type planar phyllosilicate with one tetrahedral

385   siloxane sheet and one octahedral alumina sheet (Zeitler et al., 2017). Under the same pH (= 8)

17

386   condition as considered in this work, it tends to have a neutral basal surface as atom substitutions

387   are less likely to happen. However, its edge surface can carry negative charges as the physically

388   bonded water would get deprotonated under the pH of 8 (Zeitler et al., 2017). Thus, adsorption of

389   cationic chitosan on kaolinite is expected to occur but mostly on the edge surface. PAM and MF

390   may display more adsorption on kaolinite than on Mt because of the exposed hydroxyl groups on

391   the alumina basal and edge surfaces of kaolinite, which promote hydrogen bonding. The

392   synergetic effect demonstrated in this work is expected to be present for kaolinite, since all three

393   types of polymers are expected to adsorb on it and the interactions driving adsorption are similar.

394   Illite is a dioctahedral mica-like mineral (Theng, 2012) which has similar molecular structure

395   with Mt. Its basal surface carries permanent negative charges due to atom substitutions while the

396   charges on the edge surface are pH dependent. Therefore, the synergetic polymer adsorption

397   observed for Mt is expected to be similar for illite. Slight difference might come from the fact

398   that atom substitution in Mt usually occurs only in the octahedral sheet while it can occur in both

399   tetrahedral and octahedral sheets in illite (Theng, 2012; Hao et al., 2018). Because of this, the

400   charge density on the basal surface of illite can be higher which may lead to enhanced adsorption

401   of cationic chitosan.

402   Due to the size limitation in MD simulations, it was not possible to reproduce the bulk

403   concentration of polymer molecules in experiments. In fact, typical bulk concentrations used in

404   experiments (Lu et al., 2016; Nittala et al., 2019) would correspond to at most one polymer

405   molecule in the simulation cell, which would not have allowed us to investigate the interactions

406   among the polymer molecules, a key aspect of this work. On the other hand, because this work

407   focused on polymer adsorption, the higher concentration used mimicked the fact that the

408   concentration of the polymers near the clay surface should be much higher than that in the bulk

18

409 solution. Different loadings of polymers can affect polymer adsorption. As some of the

410 experimental works suggested (Lu et al., 2016; Zhang et al., 2017), there could be an optimal

411 dosage of polymers for which the extent of flocculation was maximized. The mechanism behind

412 the observations is unclear and is a very interesting question to address in the future.

413   Furthermore, the ions included in the simulation systems were monovalent (Na^+). Multiple

414 types of ions can exist in waste-water, such as Na^+, Ca^{2+}, Mg^{2+}, Cl^-, HCO_3^-, SO_4^{2-}, NH_4^+ (Allen,

415 2008). There was evidence that divalent ions, such as Ca^{2+}, could form more stable bridges

416 between clay mineral and anionic polymers which enhanced their adsorption (Li et al., 2005). In

417 fact, in our simulations MF by themselves did not exhibit any adsorption, which appeared

418 contradictory to earlier experimental studies where MF and other anionic polymers showed

419 flocculating abilities. The presence of divalent ions in the experiments (Li et al., 2005; Lu et al.,

420 2016) could be a reason for the discrepancy; another contributing factor could be the hydroxyl

421 groups on the edge surfaces of Mt and basal/edge surfaces of kaolinite (Bish, 1993) in the

422 experiments. It is worth mentioning that some ions could also compete with polymers in the

423 adsorption and even formed surface complexes on Mt (Bourg and Sposito, 2011) that hindered

424 polymer adsorption. Effect of different ions are being investigated and will be reported elsewhere.

425   Finally, the sizes of clay mineral particles (~1 μm) and polymers (molar mass $10^{6\sim7}$ g/mol) in

426 practical settling (Wang et al., 2014) are much larger than the molecular models studied here. As

427 with any molecular simulations, the length and time scales of our simulations are limited by the

428 state-of-the-art computing capabilities. On the other hand, the atomistic simulations revealed the

429 intermolecular interactions that give rise to synergetic adsorption, which could not be obtained

430 with lab-scale resolution. The good agreement found here between mechanistic insights from

19

431   simulations and synergetic flocculation observed in experiments supports the complementarity of

432   the two approaches, which have great potential for other advanced studies in clay science.

433   **4. Conclusion**

434   Molecular dynamics simulations revealed different characteristics for the adsorptions of

435   cationic (chitosan), neutral (PAM), and anionic (MF) polymers on the negatively charged basal

436   surface of montmorillonite. When a single type of polymers was added, chitosan showed fast and

437   stable monolayer adsorption, driven by electrostatic attraction; PAM displayed weak adsorption

438   driven by hydrogen bonding, mainly in an aggregated form; and MF showed no adsorption.

439   When chitosan was added to PAM or MF, their adsorption was significantly enhanced. Chitosan

440   not only served as bridges between PAM (or MF) and montmorillonite, but also promoted direct

441   adsorption of PAM on montmorillonite. The findings correlated well with the synergetic effect

442   observed in flocculation experiments, and have direct implications on the selection of flocculants

443   as well as the design of flocculation procedure.

444   **Supporting Information**

445   **S1. Validation of force fields for clay minerals and organic molecules**

446   **S2. Partial charge calculation**

447   **S3. Additional results for the simulated systems**

448   **S4. Calculation of hydrogen bonds**

449   **Acknowledgement**

20

454 **Reference**

455 Abraham, M. J., Murtola, T., Schulz, R., Páll, S., Smith, J. C., Hess, B., Lindahl, E., 2015.

456   GROMACS: High performance molecular simulations through multi-level parallelism from

457   laptops to supercomputers. SoftwareX 1–2, 19–25.

458   https://doi.org/10.1016/j.softx.2015.06.001

459 Alamgir, A., Harbottle, D., Masliyah, J., Xu, Z., 2012. Al-PAM assisted filtration system for

460   abatement of mature fine tailings. Chem. Eng. Sci. 80, 91–99.

461   https://doi.org/10.1016/j.ces.2012.06.010

462 Allen, E.W., 2008. Process water treatment in Canada's oil sands industry: I. Target pollutants

463   and treatment objectives. J. Environ. Eng. Sci. 7, 123–138. https://doi.org/10.1139/S07-038

464 Azevedo Rios Silva, F., Araújo Sales, M.J., Ghoul, M., Chebil, L., Duarte Ramos Matos, G.,

465   Maia, E.R., 2018. Molecular dynamics simulations of montmorillonite reinforcing amylose

466   plasticized by Brazilian Cerrado oils: Polymer-clay nanocomposite. MRS Commun. 8, 266–

467   274. https://doi.org/10.1557/mrc.2018.41

468 Bakhshi, N.N., Gillies, R.G., Khare, P., 1975. Treatment of tar sands tailings with fly ash.

469   Environ. Sci. Technol. https://doi.org/10.1021/es60102a013

470 Berendsen, H.J.C., van der Spoel, D., van Drunen, R., 1995. GROMACS: a message-passing

471   parallel molecular dynamics implementation. Comput. Phys. Commun. 91, 43−56.

472   https://doi.org/10.1016/0010-4655(95)00042-E

473 Bish, D.L., 1993. Rietveld refinement of the kaolinite structure at 1.5 K. Clays Clay Miner. 41,

474   738–744. https://doi.org/10.1346/CCMN.1993.0410613

21

475   Bourg, I.C., Sposito, G., 2011. Molecular dynamics simulations of the electrical double layer on

476   smectite surfaces contacting concentrated mixed electrolyte (NaCl-CaCl2) solutions. J.

477   Colloid Interface Sci. 360, 701–715. https://doi.org/10.1016/j.jcis.2011.04.063

478   Bourg, I.C., Sposito, G., Bourg, A.C.M., 2007. Modeling the acid-base surface chemistry of

479   montmorillonite.   J.   Colloid   Interface   Sci.   312,   297–310.

480   https://doi.org/10.1016/j.jcis.2007.03.062

481   Chen, J., Min, F., Liu, L., Cai, C., 2020. Systematic exploration of the interactions between Fe-

482   doped   kaolinite   and   coal   based   on   DFT   calculations.   Fuel   266,   117082.

483   https://doi.org/10.1016/j.fuel.2020.117082

484   Cheng, H., Zhang, S., Liu, Q., Li, X., Frost, R.L., 2015. The molecular structure of kaolinite-

485   potassium acetate intercalation complexes: A combined experimental and molecular

486   dynamic   simulation   study.   Appl.   Clay   Sci.   116–117,   273–280.

487   https://doi.org/10.1016/j.clay.2015.04.008

488   Cygan, R.T., Greathouse, J.A., Heinz, H., Kalinichev, A.G., 2009. Molecular models and

489   simulations   of   layered   materials.   J.   Mater.   Chem.   19,   2470.

490   https://doi.org/10.1039/b819076c

491   Cygan, R.T., Liang, J.J., Kalinichev, A.G., 2004. Molecular models of hydroxide, oxyhydroxide,

492   and clay phases and the development of a general force field. J. Phys. Chem. B 108, 1255–

493   1266. https://doi.org/10.1021/jp0363287

494   Darden, T., York, D., Pedersen, L., 1993. Particle mesh Ewald: An N · log(N) method for Ewald

495   sums in large systems. J. Chem. Phys 98, 10089–10092. https://doi.org/10.1063/1.464397

496   Downs, R.T., Hall-Wallace, M., 2003. The American Mineralogist crystal structure database.

497   Am. Mineral. 88, 247–250.

498   Fernandes, D., Conway, W., Wang, X., Burns, R., Lawrance, G., Maeder, M., Puxty, G., 2012.

499   Protonation constants and thermodynamic properties of amines for post combustion capture

500   of CO 2. J. Chem. Thermodyn. 51, 97–102. https://doi.org/10.1016/j.jct.2012.02.031

501   Fraenkel, G., Franconi, C., 1960. Protonation of Amides. J. Am. Chem. Soc. 82, 4478–4483.

502   https://doi.org/10.1021/ja01502a010

503   Gorakhki, M.H., Bareither, C.A., 2015. Salinity effects on sedimentation behavior of kaolin,

504   bentonite, and soda ash mine tailings. Appl. Clay Sci. 114, 593–602.

505   https://doi.org/10.1016/j.clay.2015.07.018

506   Grant, H., Mctigue, P., Ward, D., 2010. The basicities of aliphatic amides. Aust. J. Chem. 36,

507   2211. https://doi.org/10.1071/ch9832211

508   Hao, Y., Yuan, L., Li, P., Zhao, W., Li, D., Lu, D., 2018. Molecular Simulations of Methane

509   Adsorption Behavior in Illite Nanopores Considering Basal and Edge Surfaces. Energy

510   Fuels 32. https://doi.org/10.1021/acs.energyfuels.8b00070

511   Hess, B., Bekker, H., Berendsen, H.J.C., Fraaije, J.G.E.M., 1997. LINCS: A linear constraint

512   solver for molecular simulations. J. Comp. Chem 18, 1463–1472.

513   https://doi.org/10.1002/(SICI)1096-987X(199709)18:12<1463::AID-JCC4>3.0.CO;2-H

514   Hockney, R.W., Goel, S.P., Eastwood, J., 1974. Quiet high resolution computer models of a

515   plasma. J. Comp. Phys 14, 148–158. https://doi.org/10.1016/0021-9991(74)90010-2

516   Hoover, W.G., 1985. Canonical dynamics: equilibrium phase-space distributions. Phys. Rev. A

517   31, 1695–1697. https://doi.org/10.1103/PhysRevA.31.1695

518   Israelachvili, J.N., 2011. Intermolecular and Surface Forces, third ed. Elsevier Inc. Waltham

519   https://doi.org/10.1016/C2011-0-05119-0

520   Ji, Y., Lu, Q., Liu, Q., Zeng, H., 2013. Effect of solution salinity on settling of mineral tailings

23

521   by polymer flocculants. Colloids Surfaces A Physicochem. Eng. Asp. 430, 29–38.

522   https://doi.org/10.1016/j.colsurfa.2013.04.006

523   Kang, X., Xia, Z., Chen, R., Sun, H., Yang, W., 2019. Effects of inorganic ions, organic

524   polymers, and fly ashes on the sedimentation characteristics of kaolinite suspensions. Appl.

525   Clay Sci. 181, 105220. https://doi.org/10.1016/j.clay.2019.105220

526   Kaniki, A.T., Tumba, K., 2019. Management of mineral processing tailings and metallurgical

527   slags of the Congolese copperbelt: Environmental stakes and perspectives. J. Clean. Prod.

528   210, 1406–1413. https://doi.org/10.1016/j.jclepro.2018.11.131

529   Kim, S., Chen, J., Cheng, T., Gindulyte, A., He, J., He, S., Li, Q., Shoemaker, B.A., Thiessen,

530   P.A., Yu, B., Zaslavsky, L., Zhang, J., Bolton, E.E., 2019. PubChem 2019 update: Improved

531   access to chemical data. Nucleic Acids Res. 47, D1102–D1109.

532   https://doi.org/10.1093/nar/gky1033

533   Li, H., Long, J., Xu, Z., Masliyah, J.H., 2005. Synergetic Role of Polymer Flocculant in Low-

534   Temperature Bitumen Extraction and Tailings Treatment. Energy Fuels 19, 936–943.

535   https://doi.org/10.1021/ef049744e

536   Li, P., Khan, M.A., Xia, M., Lei, W., Zhu, S., Wang, F., 2019. Efficient preparation and

537   molecular dynamic (MD) simulations of Gemini surfactant modified layered

538   montmorillonite to potentially remove emerging organic contaminants from wastewater.

539   Ceram. Int. 45, 10782–10791. https://doi.org/10.1016/j.ceramint.2019.02.152

540   Liu, Y., Lv, C., Ding, J., Qian, P., Zhang, X., Yu, Y., Ye, S., Chen, Y., 2016. The use of the

541   organic-inorganic hybrid polymer Al(OH)3-polyacrylamide to flocculate particles in the

542   cyanide tailing suspensions. Miner. Eng. 89, 108–117.

543   https://doi.org/10.1016/j.mineng.2016.01.018

24

544   Long, J., Li, H., Xu, Z., Masliyah, J.H., 2006. Role of colloidal interactions in oil sand tailings

545   treatment. AIChE J. 52, 371–383. https://doi.org/10.1002/aic.10603

546   Lu, H., Wang, Y., Li, L., Kotsuchibashi, Y., Narain, R., Zeng, H., 2015. Temperature- and pH-

547   Responsive Benzoboroxole-Based Polymers for Flocculation and Enhanced Dewatering of

548   Fine   Particle   Suspensions.   ACS   Appl.   Mater.   Interfaces   7,   27176–27187.

549   https://doi.org/10.1021/acsami.5b09874

550   Lu, H., Xiang, L., Cui, X., Liu, J., Wang, Y., Narain, R., Zeng, H., 2016. Molecular Weight

551   Dependence of Synthetic Glycopolymers on Flocculation and Dewatering of Fine Particles.

552   Langmuir 32, 11615–11622. https://doi.org/10.1021/acs.langmuir.6b03072

553   Lu, Q., Yan, B., Xie, L., Huang, J., Liu, Y., Zeng, H., 2016. A two-step flocculation process on

554   oil sands tailings treatment using oppositely charged polymer flocculants. Sci. Total

555   Environ. 565, 369–375. https://doi.org/10.1016/j.scitotenv.2016.04.192

556   Frisch, M. J., Trucks, G. W., Schlegel, H. B., Scuseria, G. E., Robb, M. A., Cheeseman, J. R.,

557   Scalmani, G., Barone, V., Petersson, G. A., Nakatsuji, H., Li, X., Caricato, M., Marenich, A.

558   V., Bloino, J., Janesko, B. G., Gomperts, R., Mennucci, B., Hratchian, H. P., Ortiz, J. V.,

559   Izmaylov, A. F., Sonnenberg, J. L., Williams-Young, D., Ding, F., Lipparini, F., Egidi, F.,

560   Goings, J., Peng, B., Petrone, A., Henderson, T., Ranasinghe, D., Zakrzewski, V. G., Gao, J.,

561   Rega, N., Zheng, G., Liang, W., Hada, M., Ehara, M., Toyota, K., Fukuda, R., Hasegawa, J.,

562   Ishida, M., Nakajima, T., Honda, Y., Kitao, O., Nakai, H., Vreven, T., Throssell, K.,

563   Montgomery, J. A., Jr., Peralta, J. E., Ogliaro, F., Bearpark, M. J., Heyd, J. J., Brothers, E.

564   N., Kudin, K. N., Staroverov, V. N., Keith, T. A., Kobayashi, R., Normand, J.,

565   Raghavachari, K., Rendell, A. P., Burant, J. C., Iyengar, S. S., Tomasi, J., Cossi, M., Millam,

566   J. M., Klene, M., Adamo, C., Cammi, R., Ochterski, J. W., Martin, R. L., Morokuma, K.,

25

567   Farkas, O., Foresman, J. B., Fox, D. J., 2016. Gaussian 16 Revision B. 01. Wallingford CT.

568   Miyamoto, S., Kollman, P.A., 1992. SETTLE: An analytical version of the SHAKE and

569   RATTLE algorithms for rigid water models. J. Comp. Chem 13, 952–962.

570   https://doi.org/10.1002/jcc.540130805

571   Molatlhegi, O., Alagha, L., 2017. Adsorption characteristics of chitosan grafted copolymer on

572   kaolin. Appl. Clay Sci. 150, 342–353. https://doi.org/10.1016/j.clay.2017.09.032

573   Moreno, L., Neretnieks, I., 2006. Long-term environmental impact of tailings deposits.

574   Hydrometallurgy 83, 176–183. https://doi.org/10.1016/j.hydromet.2006.03.052

575   Nasim, T., Pal, A., Bandyopadhyay, A., 2018. Flocculation of aqueous kaolin suspension using a

576   biodegradable flocculant system of poly (vinyl alcohol)-Acacia nilotica gum blends. Appl.

577   Clay Sci. 152, 83–92. https://doi.org/10.1016/j.clay.2017.10.035

578   Ngnie, G., Baitan, D., Dedzo, G.K., Detellier, C., 2018. Sedimentation of fine particles of

579   kaolinite and polymer-coated kaolinite in cyclohexane: Implications for fines removal from

580   extracted bitumen in non-aqueous processes. Fuel 234, 218–224.

581   https://doi.org/10.1016/j.fuel.2018.07.032

582   Nittala, A.K., Gumfekar, S.P., Soares, J.B.P., 2019. Multifunctional CO_2-switchable polymers

583   for the flocculation of oil sands tailings. J. Appl. Polym. Sci. 136, 1–9.

584   https://doi.org/10.1002/app.47578

585   Nosé, S., 1984. A molecular dynamics method for simulations in the canonical ensemble. Mol.

586   Phys 52, 255–268. https://doi.org/10.1080/00268978400101201

587   Omotoso, O.E., Mikula, R.J., 2004. High surface areas caused by smectitic interstratification of

588   kaolinite and illite in Athabasca oil sands. Appl. Clay Sci. 25, 37–47.

589   https://doi.org/10.1016/j.clay.2003.08.002

26

590   Oostenbrink, C., Villa, A., Mark, A.E., Van Gunsteren, W.F., 2004. A biomolecular force field

591   based on the free enthalpy of hydration and solvation: The GROMOS force-field parameter

592   sets 53A5 and 53A6. J. Comput. Chem. 25, 1656–1676. https://doi.org/10.1002/jcc.20090

593   Parrinello, M., Rahman, A., 1981. Polymorphic transitions in single crystals: A new molecular

594   dynamics method. J. Appl. Phys 52, 7182−7190. https://doi.org/10.1063/1.328693

595   Pouvreau, M., Greathouse, J.A., Cygan, R.T., Kalinichev, A.G., 2017. Structure of Hydrated

596   Gibbsite and Brucite Edge Surfaces: DFT Results and Further Development of the ClayFF

597   Classical Force Field with Metal-O-H Angle Bending Terms. J. Phys. Chem. C 121, 14757–

598   14771. https://doi.org/10.1021/acs.jpcc.7b05362

599   Pronk, S., Páll, S., Schulz, R., Larsson, P., Bjelkmar, P., Apostolov, R., Shirts, M. R., S., J. C.,

600   Kasson, P. M., van der Spoel, D., Hess, B., Lindahl, E., 2013. GROMACS 4.5: a

601   highthroughput and highly parallel open source molecular simulation toolkit.

602   Bioinformatics 29, 845–854. https://doi.org/10.1093/bioinformatics/btt055

603   Razmimanesh, F., Amjad-Iranagh, S., Modarress, H., 2015. Molecular dynamics simulation

604   study of chitosan and gemcitabine as a drug delivery system. J. Mol. Model. 21.

605   https://doi.org/10.1007/s00894-015-2705-2

606   Ren, B., Min, F., Liu, L., Chen, J., Liu, C., Lv, K., 2020. Adsorption of different PAM structural

607   units on kaolinite (0 0 1) surface: Density functional theory study. Appl. Surf. Sci. 504.

608   https://doi.org/10.1016/j.apsusc.2019.144324

609   Robert, T., Mercer, S.M., Clark, T.J., Mariampillai, B.E., Champagne, P., Cunningham, M.F.,

610   Jessop, P.G., 2012. Nitrogen-containing polymers as potent ionogens for aqueous solutions

611   of switchable ionic strength: application to separation of organic liquids and clay particles

612   from water. Green Chem. 14, 3053. https://doi.org/10.1039/c2gc36074h

27

613   Schüttelkopf, A.W., Van Aalten, D.M.F., 2004. PRODRG: A tool for high-throughput

614   crystallography of protein-ligand complexes. Acta Crystallogr. Sect. D Biol. Crystallogr. 60,

615   1355–1363. https://doi.org/10.1107/S0907444904011679

616   Shaikh, S.M.R., Nasser, M.S., Magzoub, M., Benamor, A., Hussein, I.A., El-Naas, M.H.,

617   Qiblawey, H., 2018. Effect of electrolytes on electrokinetics and flocculation behavior of

618   bentonite-polyacrylamide dispersions. Appl. Clay Sci. 158, 46–54.

619   https://doi.org/10.1016/j.clay.2018.03.017

620   Song, K., Sandí, G., 2001. Characterization of montmorillonite surfaces after modification by

621   organosilane. Clays Clay Miner. 49, 119–125.

622   https://doi.org/10.1346/CCMN.2001.0490202

623   Suter, J.L., Coveney, P. V., Anderson, R.L., Greenwell, H.C., Cliffe, S., 2011. Rule based design

624   of clay-swelling inhibitors. Energy Environ. Sci. 4, 4572–4586.

625   https://doi.org/10.1039/c1ee01280k

626   Theng, B.K.G., 2012. Formation and properties of clay-polymer complexes. Elsevier,

627   Developmnets of Clay Science, Volume 4, Amsterdam https://doi.org/10.1016/B978-

628   075068620-4.50036-8

629   Viani, A., Gualtieri, A.F., Artioli, G., 2002. The nature of disorder in montmorillonite by

630   simulation of X-ray powder patterns. Am. Mineral. 87, 966–975.

631   Wang, C., Han, C., Lin, Z., Masliyah, J., Liu, Q., Xu, Z., 2016. Role of Preconditioning Cationic

632   Zetag Flocculant in Enhancing Mature Fine Tailings Flocculation. Energy and Fuels 30,

633   5223–5231. https://doi.org/10.1021/acs.energyfuels.6b00108

634   Wang, C., Harbottle, D., Liu, Q., Xu, Z., 2014. Current state of fine mineral tailings treatment: A

635   critical review on theory and practice. Miner. Eng. 58, 113–131.

28

636   https://doi.org/10.1016/j.mineng.2014.01.018

637   Wang, Q.Z., Chen, X.G., Liu, N., Wang, S.X., Liu, C.S., Meng, X.H., Liu, C.G., 2006.

638   Protonation constants of chitosan with different molecular weight and degree of

639   deacetylation.   Carbohydr.   Polym.   65,   194–201.

640   https://doi.org/10.1016/j.carbpol.2006.01.001

641   Wang, X.W., Feng, X., Xu, Z., Masliyah, J.H., 2010. Polymer aids for settling and filtration of

642   oil sands tailings. Can. J. Chem. Eng. 88, 403–410. https://doi.org/10.1002/cjce.20283

643   Wang, Y., Wohlert, J., Bergenstråhle-Wohlert, M., Tu, Y., Ågren, H., 2015. Molecular

644   mechanisms for the adhesion of chitin and chitosan to montmorillonite clay. RSC Adv. 5,

645   54580–54588. https://doi.org/10.1039/c5ra06424d

646   Watson, A.H., Corser, P.G., Garces Pardo, E.E., Lopez Christian, T.E., Vandekeybus, J., 2010. A

647   comparison of alternative tailings disposal methods—the promises and realities. In: R

648   Jewell & AB Fourie (eds) Proceedings of the First International Seminar on the Reduction

649   of Risk in the Management of Tailings and Mine Waste, Australian Centre for

650   Geomechanics, Perth, pp. 499-514. https://doi.org/10.36487/ACG_rep/1008_41_Watson

651   Wei, Q., Wang, Y., Wang, S., Zhang, Y., Chen, X., 2017. Investigating the properties and

652   interaction mechanism of nano-silica in polyvinyl alcohol/polyacrylamide blends at an

653   atomic   level.   J.   Mech.   Behav.   Biomed.   Mater.   75,   529–537.

654   https://doi.org/10.1016/j.jmbbm.2017.08.027

655   Willemsen, J.A.R., Myneni, S.C.B., Bourg, I.C., 2019. Molecular Dynamics Simulations of the

656   Adsorption of Phthalate Esters on Smectite Clay Surfaces. J. Phys. Chem. C 123, 13624–

657   13636. https://doi.org/10.1021/acs.jpcc.9b01864

658   Yang, Z., Shang, Y., Lu, Y., Chen, Y., Huang, X., Chen, A., Jiang, Y., Gu, W., Qian, X., Yang,

659   H., Cheng, R., 2011. Flocculation properties of biodegradable amphoteric chitosan-based

660   flocculants. Chem. Eng. J. 172, 287–295. https://doi.org/10.1016/j.cej.2011.05.106

661   Zeitler, T.R., Greathouse, J.A., Cygan, R.T., Fredrich, J.T., Jerauld, G.R., 2017. Molecular

662   Dynamics Simulation of Resin Adsorption at Kaolinite Edge Sites: Effect of Surface

663   Deprotonation on Interfacial Structure. J. Phys. Chem. C 121, 22787–22796.

664   https://doi.org/10.1021/acs.jpcc.7b06688

665   Zhang, D., Thundat, T., Narain, R., 2017. Flocculation and dewatering of mature fine tailings

666   using temperature-responsive cationic polymers. Langmuir 33, 5900–5909.

667   https://doi.org/10.1021/acs.langmuir.7b01160

668   Zvulunov, Y., Ben-Barak-Zelas, Z., Fishman, A., Radian, A., 2019. A self-regenerating clay-

669   polymer-bacteria composite for formaldehyde removal from water. Chem. Eng. J. 374,

670   1275–1285. https://doi.org/10.1016/j.cej.2019.06.017

671

Table 1. Details of Simulated Systems

system name	polymers	number of Na$^+$	simulated time
Mt-H$_2$O	0	120	2.5 ns
Mt-CT	chitosan (3×2×2)	0	7 ns
Mt-PAM	PAM (3×2×2)	120	110 ns
Mt-MF	MF (3×2×2)	156	50 ns
Mt-(CT-PAM)	chitosan (3×1×2) + PAM (3×1×2)	60	80 ns
Mt-(CT-MF)	chitosan (3×1×2) + MF (3×1×2)	78	80 ns
(Mt-CT)-MF	Mt-CT + MF (3×2×2)	0 → 36	80 ns
(Mt-CT)-PAM	Mt-CT + PAM (3×2×2)	0 → 0	80 ns
(Mt-PAM)-CT	Mt-PAM + chitosan (3×2×2)	120 → 0	80 ns
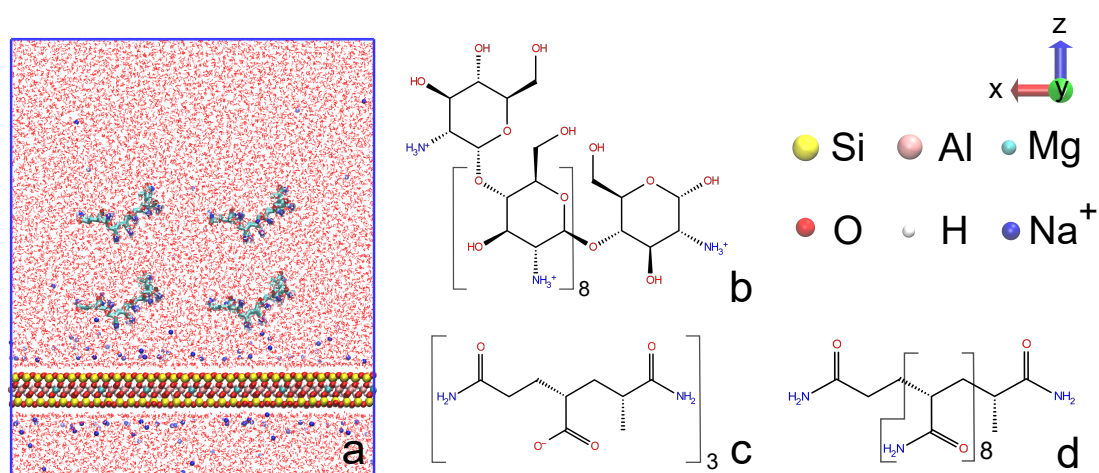
Figure 1. Initial configuration of system Mt-PAM (a), chitosan (b), MF 1011 (c), and PAM (d). In (a), the Mt supercell is represented by ball and stick. PAM is in licorice representation. Water as solvent is in line representation.
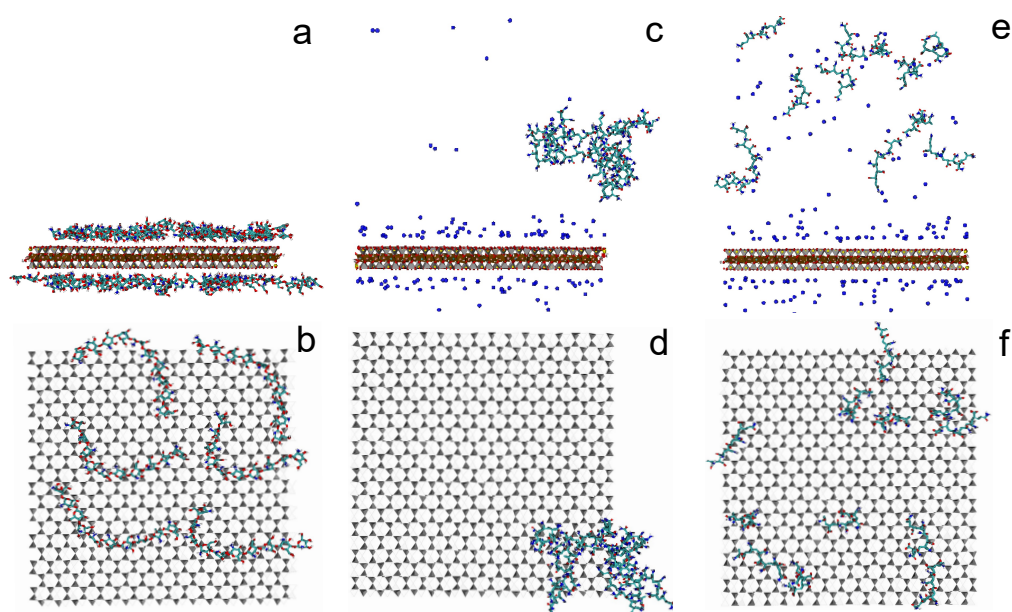
Figure 2. Snapshots of the final configuration of systems Mt-CT (a, b), Mt-PAM (c, d), and Mt-MF (e, f). Side view (a, c, e) and top view (b, d, f) are shown for each system. In top view, the alumina octahedron in Mt is not displayed, and water as well as ions are removed for clarity.
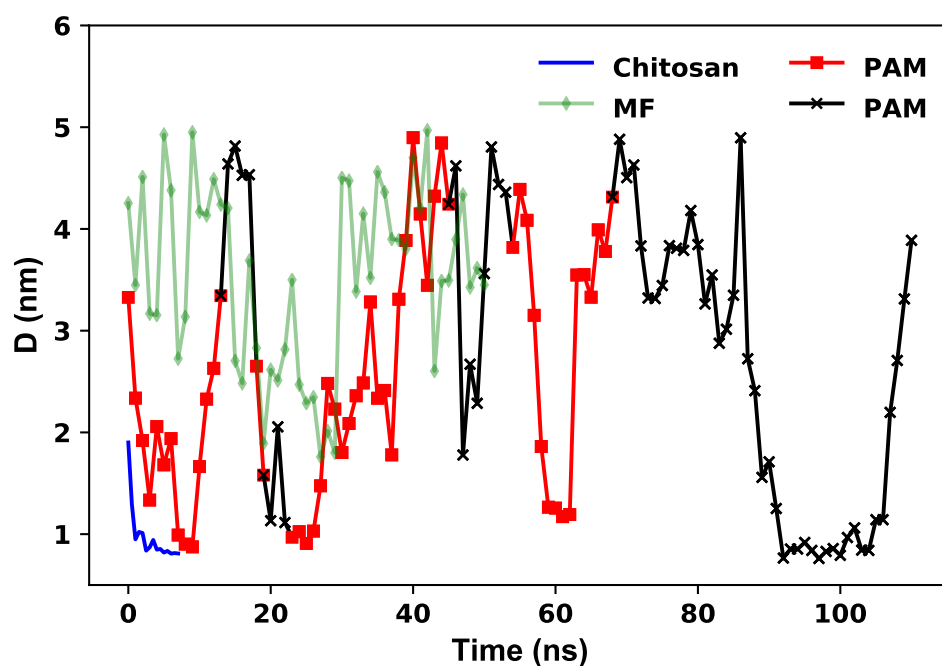
Figure 3. Vertical distances (D) between COG of Mt and COG of one representative chitosan molecule in system Mt-CT, one representative MF molecule in Mt-MF, and one representative PAM molecule in Mt-PAM, plotted against simulation time. For the representative PAM molecule in Mt-PAM, the "×" symbol corresponds to it being aggregated with other PAM molecules while the square symbol corresponds to it being in an un-aggregated state.
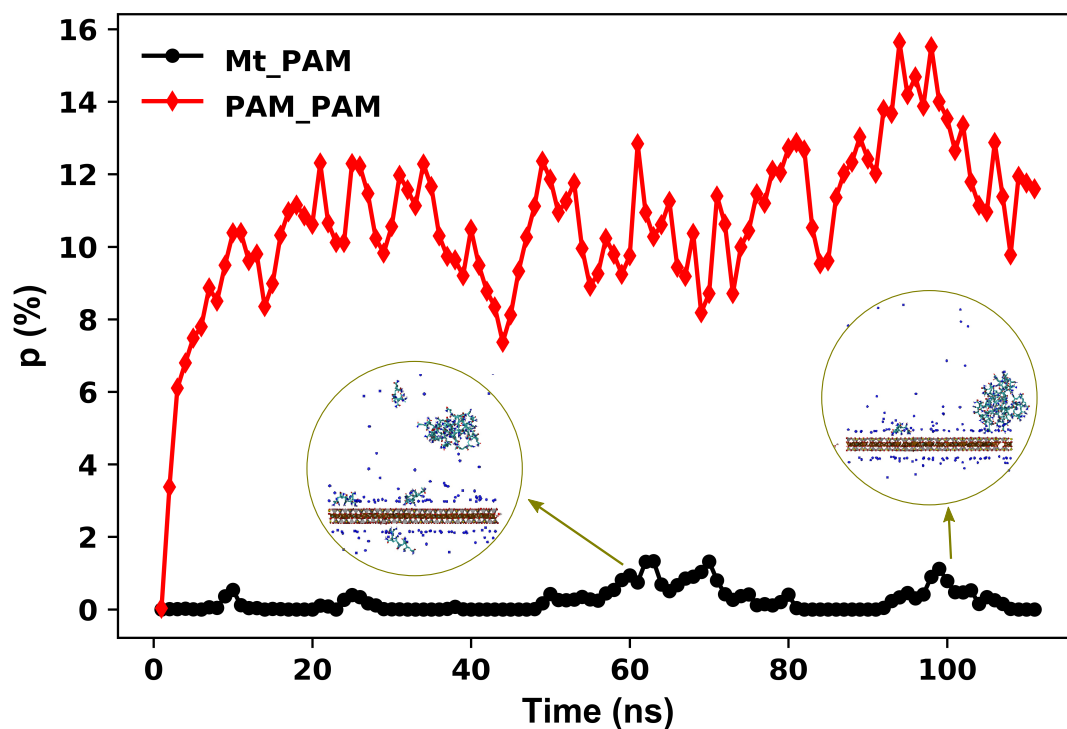
Figure 4. Vertical distances (D) between COG of Mt and COG of one representative chitosan molecule in system Mt-CT, one representative MF molecule in Mt-MF, and one representative PAM molecule in Mt-PAM, plotted against simulation time. For the representative PAM molecule in Mt-PAM, the "×" symbol corresponds to it being aggregated with other PAM molecules while the square symbol corresponds to it being in an un-aggregated state.
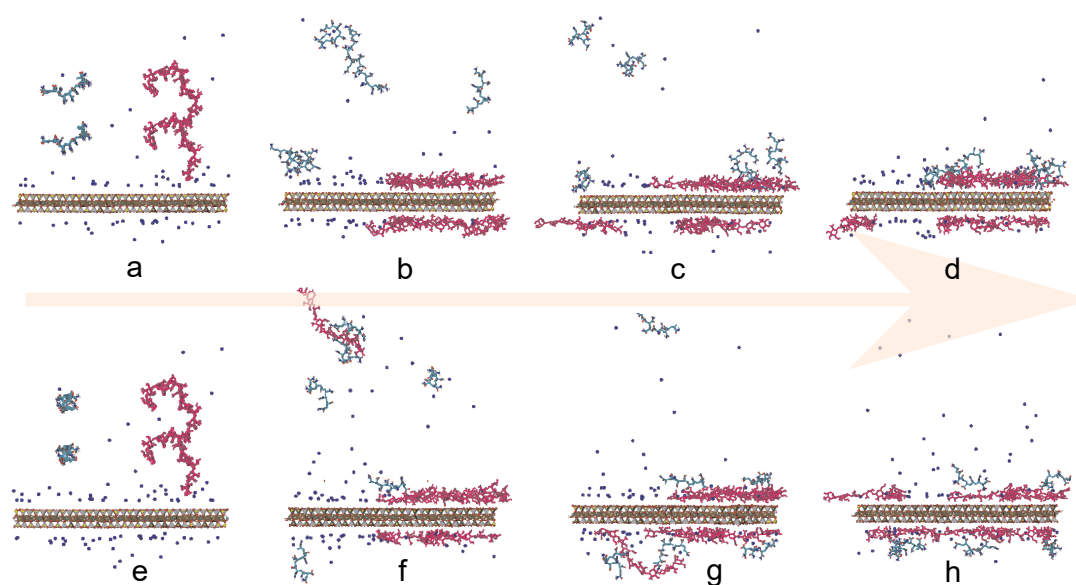
Figure 5. Snapshots of system Mt-(CT-PAM) at $t =$ (a) 0 ns, (b) 3 ns, (c) 31 ns and (d) 80 ns; and of system Mt-(CT-MF) at $t =$ (e) 0 ns, (f) 10 ns, (g) 40 ns and (h) 80 ns. At $t = 0$ ns, chitosan molecules are on the right while PAM and MF molecules are on the left. Water is removed for clarity.
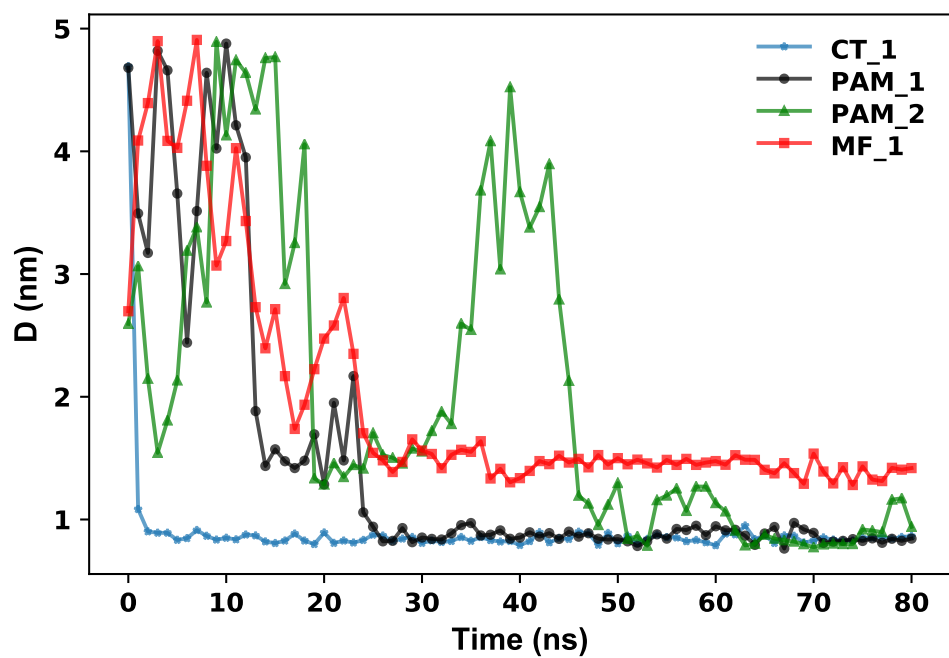
Figure 6. Vertical distances (D) between COG of Mt and COG of representative polymer molecules, plotted against simulation time.
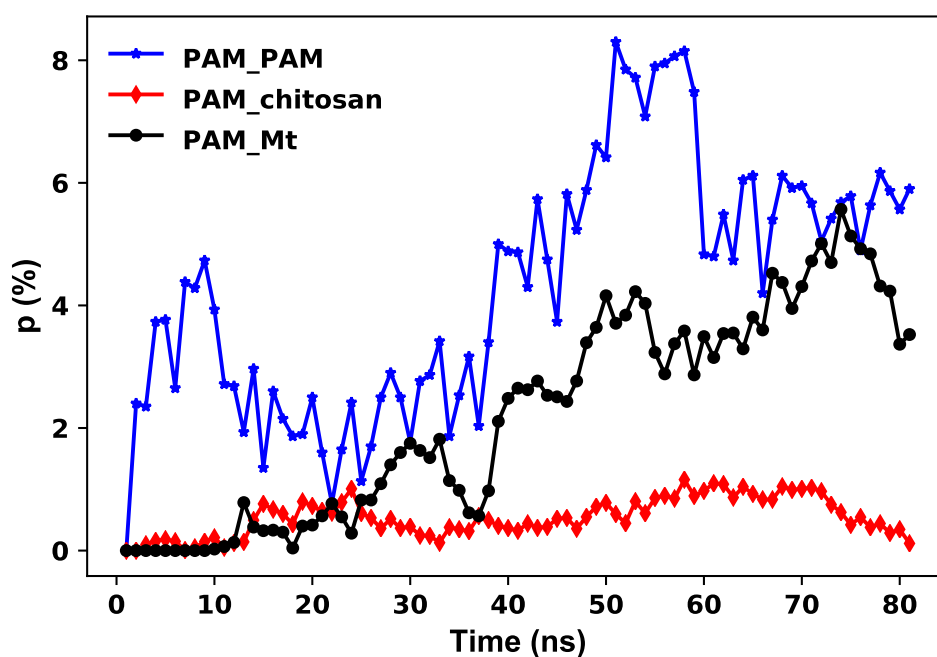
Figure 7. Percentage of available donor/acceptor pairs that contributed to H-bonding, among PAM molecules, between PAM and chitosan, and between PAM and Mt in system Mt-(CT-PAM).
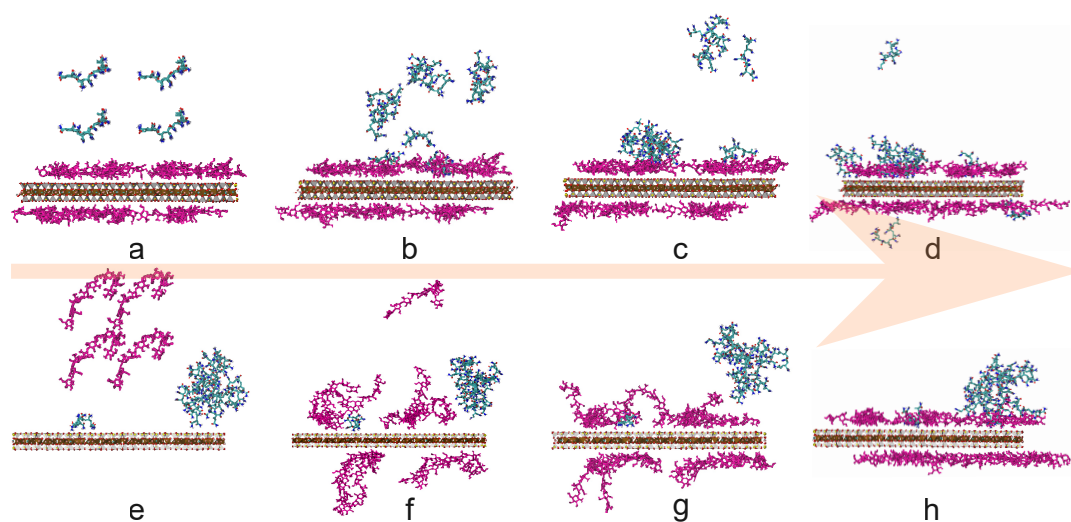
Figure 8. Snapshots of system (Mt-CT)-PAM at $t =$ (a) 0 ns, (b) 3 ns, (c) 20 ns, and (d) 80 ns; and of system (Mt-PAM)-CT at $t =$ (e) 0 ns, (f) 0.2 ns, (g) 0.6 ns, and (h) 80 ns. The $3 \times 2 \times 2$ arrays of molecules above Mt in (a) and (e) correspond to PAM and chitosan, respectively. Water is removed for clarity.
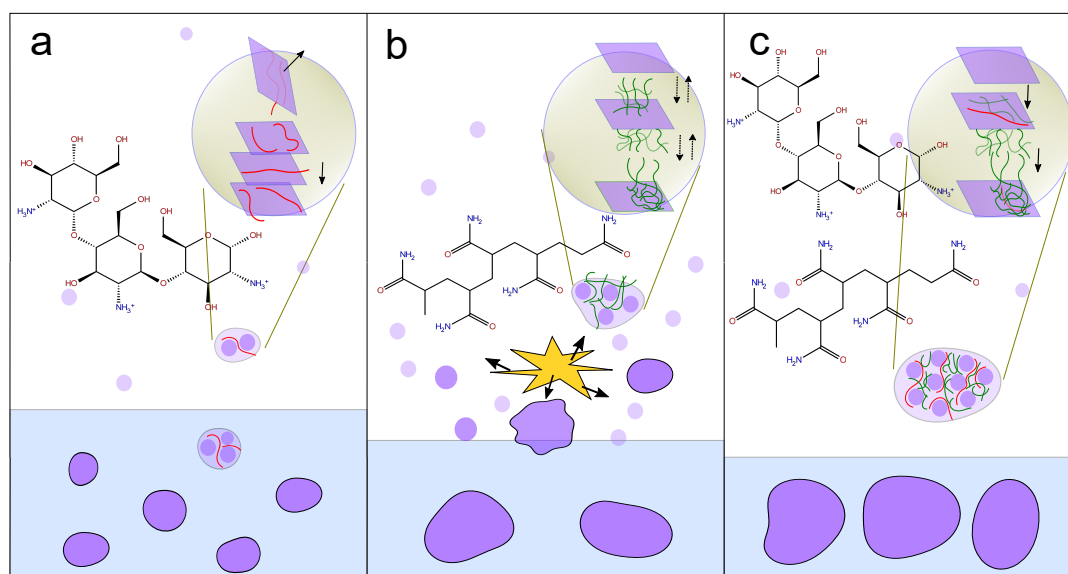
Figure 9. Proposed mechanism for the macroscopic flocculation of Mt by the addition of chitosan (a), PAM (b), chitosan and PAM (c). Plates represent the clay mineral particles; chitosan and PAM are represented by strings. Refer to Figure 1 for detailed molecular structures.